Multi-Body and Unsteady Rotorcraft/Slung Load Modeling and Simulation

Chengjian He, JingGen Zhao, and Jan Goericke

Advanced Rotorcraft Technology, Inc.
1330 Charleston Road
Mountain View, CA 94043, U.S.A.
he@flightlab.com

Key words: rotorcraft/slung load simulation, rotorcraft/slung load dynamics, slung load aerodynamics

Abstract

This paper summarizes the formulation and the solution technique that were developed for high fidelity rotorcraft/slung load modeling and simulation. The modeling tool that was built was based on geometrically accurate multi-body dynamics and unsteady slung load aerodynamics formulations. The modeling tool was integrated in a comprehensive rotorcraft simulation program, FLIGHTLAB, and can be applied to simulate all existing arbitrary helicopter/slung load configurations, including multiple sling cables, multi-stage sling cables, multiple sling hooks, and multiple loads. The simulation tool was validated using a UH-60L/CONEX load configuration. Good agreement was obtained with the flight test measured data.

1 Introduction

Slung load handling is a unique capability of rotorcraft widely applied in support of cargo transportation, rescue, and the special construction in areas where no other air or ground vehicles can operate. The presence of a sling load can degrade rotorcraft handling qualities and reduce the flight envelope. An accurate assessment of the sling load dynamic stability and the operational envelope is required for a safe flight. A validated rotorcraft/slung load simulation can significantly reduce cost and enhance the flight safety of such operations. The modeling and analysis of rotorcraft slung load operations is, however, a complicated task involving coupling of the nonlinear dynamics, aerodynamics, and controls. The challenging aspects of current slung load simulation and analysis include modeling of the highly nonlinear dynamics and unsteady aerodynamics and development of an accurate

trim, stability, and control response solution for the coupled rotorcraft/slung load multi-body dynamic system. An accurate model of the rotorcraft/slung load system requires that both the inertia and the aerodynamics of the slung load and its dynamic interaction with the rotorcraft be properly addressed.

Cicolani, et al (Refs. [1], [2], and [3]) developed the simulation model of the helicopter/slung load system by using several rigid bodies connected by elastic straight-line cables. The equations of motion for the entire helicopter/slung load system were derived from the Newton-Euler rigid body equations using the generalized velocity coordinates. Following the explicit constraint method, which utilizes d'Alembert's principle, the system is partitioned into coordinates such that the motion due to the cable stretching is separated from that due to the rigid body coupled dynamics. The derived equations of motion were implemented in the GENHEL simulation program and simulation results were compared with flight test data in frequency domain. Promising results were shown in the correlation between the simulation and the flight test. The work of Refs. [1] to [3] provided valuable insight into the complicated helicopter/slung load dynamic phenomena and has enriched our understanding of the problem.

Instead of deriving the dynamic equations for a given rotorcraft/slung load configuration which may vary significantly from one configuration to another, current development adopts the modern multi-body dynamics formulation. Under the multi-body dynamics approach, the modeling elements were first developed. The modeling library thus built contains a set of modules for the external slung or towed load dynamics and aerodynamics simulation. Once the modeling element library has been established, the next essential step is the simulation model assembly for any arbitrary rotorcraft/slung load configuration. This was accomplished through FLIGHTLAB (Ref.[4]) object oriented modeling environment. In the FLIGHTLAB simulation model assemble process, the modeling elements are integrated through enforcing the element boundary conditions at each element connection node. The rotorcraft/slung load model thus assembled can be arbitrary slung load configurations including the models for multiple cables, multi-stage sling cables, and multi-hooks. More sophisticated configurations can also be addressed that include the models with a sling space bar and/or a sling swivel.

A previous paper summarized the study that investigated the potential for applying the FLIGHTLAB modeling tool for a simulation-based Airworthness certification of external sling load (Ref. [5]). Results of the simulation validation and related flight tests were also discussed in the Ref. [5]. This paper will presents the helicopter/slung load model formulation and solution technique that were used for the rotorcraft/slung load dynamics modeling tool development.

2 Rotorcraft/Slung Load Dynamics

A rotorcraft/slung load configuration is a two body dynamic system. An accurate representation of the rotorcraft/slung load dynamics requires knowledge of the exact position of the interconnected subsystem elements. The multi-body dynamics formulation adopted in FLIGHTLAB best suits for such applications.

2.1 Model Building Blocks

The complex dynamics model of rotorcraft/slung load configuration is built by assembling the basic modeling elements. The modeling elements act as the model building blocks of the simulation. The elements are connected to one another by enforcing the element interface force boundary conditions and motion compatibility.

2.1.1 Reference Frame

In formulating the modeling elements, an element local coordinate system is first defined which is a set of orthogonal, right-hand, Cartesian axes used to describe vector quantities including position, velocity, acceleration, forces and moments. For each element, a reference frame is also established which is a fictitious rigid body used to describe the motion and the orientation of a system. For a global reference, an inertial reference frame is used in which the generalized Newton's second law can be applied. The global inertial frame is established as a common reference for all the modeling elements. With the global reference frame, the relative motion between the elements can be calculated. The orientation of each dynamic element is computed during the simulation by a local frame transformation with respect to the global inertial frame. With the element local frame transformation, the relative orientation of the each element can be obtained. The relative orientation variables are the Euler angles (ϕ, θ, ψ) with which a transformation matrix from inertial to the local element frame can be formed, i.e.,

$$T_{p/i} = \begin{bmatrix} \cos\psi\cos\theta & \sin\psi\cos\theta & -\sin\theta \\ -\sin\psi\cos\phi + \cos\psi\sin\theta\sin\phi & \cos\psi\cos\phi + \sin\psi\sin\theta\sin\phi & \cos\theta\sin\phi \\ \sin\psi\sin\phi + \cos\psi\sin\theta\cos\phi & -\cos\psi\sin\phi + \sin\psi\sin\theta\cos\phi & \cos\theta\cos\phi \end{bmatrix}$$

This transformation is used to transform vector quantities such as a velocity vector from one coordinate system to another. Successive transformations may be represented by a single transformation. The total transformation from inertial to the local element frame is the product of all the transformations.

2.1.2 Modeling Elements

Example modeling elements used for slung load modeling are conventional springs, dampers, cables, hinges, rigid translation and rotation, rigid bar and elastic beams, 3 DOF (translation only) point mass, 6 DOF nonlinear rigid body, etc. The analytical formulas for these basic elements are derived from physical laws. The spring/damper element can be either linear or nonlinear. For the nonlinear spring/damper model, the spring stiffness and damping coefficients are tabulated as function of the spring deformation and damper relative velocity. The cable element is the special case of the nonlinear spring/damper where the tension only exists in stretching. There are also special element developed for slung load modeling. These include space bar and swivel modeling elements.

The *space bar* is a rigid beam in the sling cable configuration which connects two free stage nodes. It is utilized to stabilize the slung load, separate cables, and offload the sling hooks. The space bar model was implemented using a translation component with distributed mass properties. The space bar has five degrees of freedom, which include

the three translational degrees of freedom as well as the pitch and yaw motions. Figure 1 illustrates the two-stage sling cable configuration with a single space bar. The space bar model presents an additional structural modeling element for sling cable configurations.

Swivel model To prevent sling cables from winding, swivels are often used in both the one-stage and two-stage slung load configurations. For simulation, the swivel is modeled as a rotation torsional spring-damper element. which models a hinge with both a torsional spring and a torsional damper about a single axis. By setting the spring and damper properties to zero, it can only pass the forces and alleviates all the moments. A two-stage slung load configuration with the torsional spring-damper component is shown in Fig. 2, where upstream of the swivel is the "free" node (Node 2 in the plot) and downstream of the swivel are the four cables connected to the CONEX slung load as shown in the figure.

2.1.3 Dynamic Model Assembly

To facilitate the process of assembling system dynamics models from the basic modeling elements, FLIGHTLAB provides utilities to automate the model assembly process. The utilities include the initialization of the data connections between the basic modeling elements and the assembly of system matrices for the solution of nonlinear dynamic equations. This flexibility has also been incorporated into the solution architecture. It allows the user to perform either an iterative solution between the subsystems or a simultaneous solution on the overall system that is often crucial for some highly coupled interdisciplinary simulations.

3 Arbitrary Sling Load Configuration

The multi-body approach in FLIGHTLAB provides modeling flexibility that facilitates the development of slung load dynamic models constructed with arbitrary sling cable configurations. Fig. 3 shows various sling configurations that can be supported by the current FLIGHTLAB simulation. The complexity of the slung load model increases with the number of sling stages. The stages in multiple sling stage configurations are interconnected by one or more nodes with translational degrees of freedom.

4 Unsteady Slung Load Aerodynamics

The slung load aerodynamics is another important aspect of coupled rotorcraft/slung load model development. This is especially the case when the slung load encounters rotor or airframe aerodynamic interference or when the aircraft is at higher flight speeds. The rotor and airframe aerodynamic interference effect becomes more critical when the slung load weight is light and operates in close proximity to the rotorcraft. The development of FLIGHTLAB slung load airloads models included the calculation of the nonlinear quasi-steady 3-D body airloads and a perturbational state space formulation for unsteady slung load airloads. The slung load airloads model also considers the effects of rotor interference on the slung load airloads calculation.

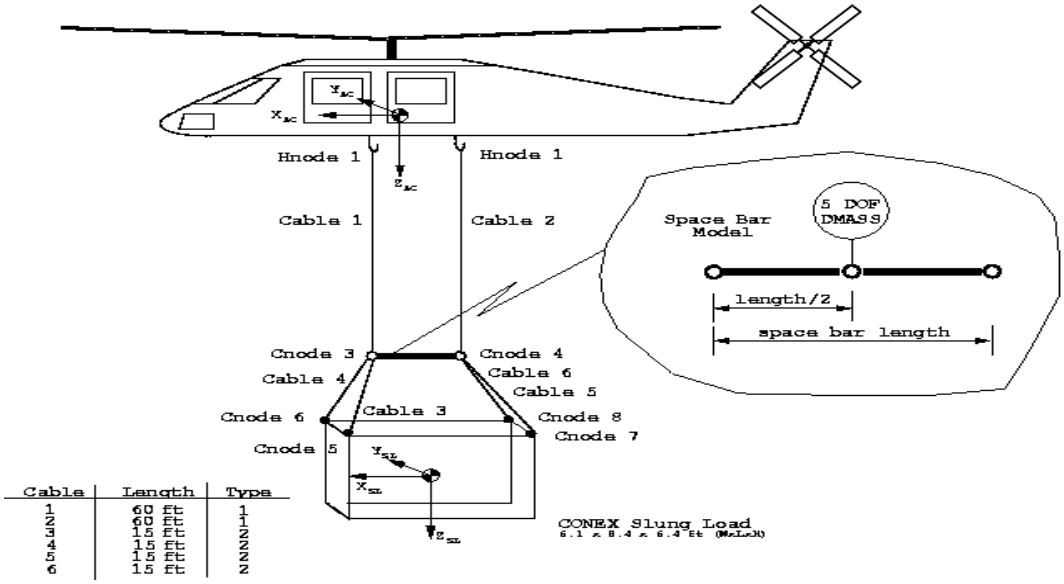

Cable	Length	Type
1	60 ft	1
2	60 ft	1
3	15 ft	2
4	15 ft	2
5	15 ft	2
6	15 ft	2

Figure 1: Space bar model

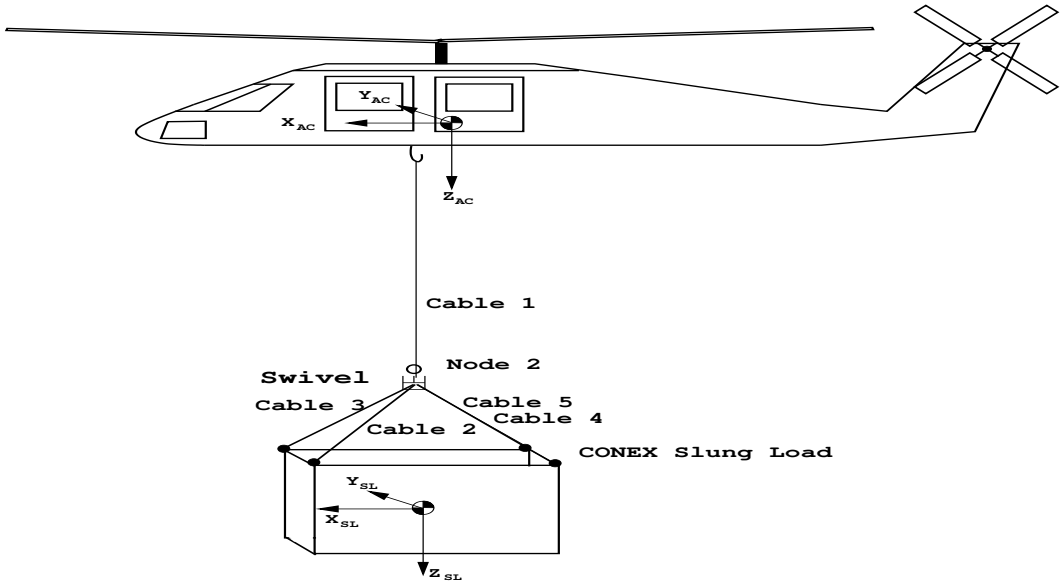

Figure 2: Swivel model

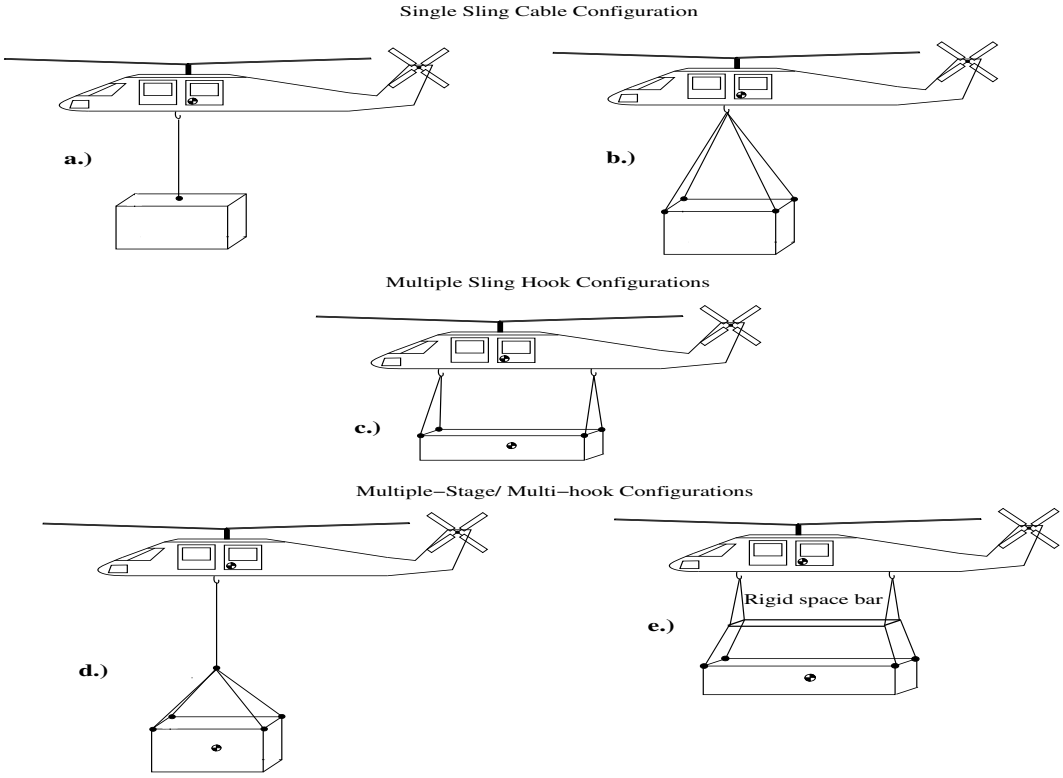

Figure 3: Various sling configurations supported by FLIGHTLAB simulation

4.1 Nonlinear Quasi-Steady Slung Load Airloads

The quasi-steady airloads acting on the slung load were computed via table lookup. The airloads model computes the airloads from the aerodynamic coefficients expressed in the wind frame as a function of body angle of attack, sideslip angle, and dynamic pressure. The airloads are then transformed to the body-fixed reference frame for simulation.

The body relative air velocity, expressed in the parent coordinate system, is computed from the vector sum of the motion of the parent reference frame, the wind, and the total induced velocity including interference. The parent coordinate system is defined as 'x' forward, 'y' to the right, and 'z' downward. The wind and the total induced velocity for the relative airspeed calculation are expressed in the inertial coordinate system. The data tables for the aerodynamic force and moment coefficients are defined in the wind axes. The force coefficients are normalized by the reference area and the dynamic pressure. The moment coefficients are normalized by the reference length in addition to the dynamic pressure and the reference area.

The total air velocity expressed in the parent coordinate system is computed as

$$v^p_{totair} = -[v^p_{p/i} + T_{p/i}(v^i_{wind} + v^i_{induced})]$$

The three components of the total air velocity are v_x, v_y, and v_z. The angles of attack and sideslip are computed as

$$\alpha = \arctan\left(\frac{-v_z}{|v_x|}\right)$$

$$\beta = \arctan\left(\frac{-v_y}{sign(v_{xz}, -v_x)}\right)$$

where, v_{xz}, denotes the air velocity in the xz-plane which is computed as

$$v_{xz} = \sqrt{v_x^2 + v_z^2}$$

The aerodynamic coefficients in the wind tunnel convention (lift (c_l), side force (c_y), drag (c_d), roll moment (c_r, '+' along body-x axis), pitch moment (c_m), and yaw moment (c_n, '+' along body-z axis)) are computed via table lookup with respect to the angle of attack and sideslip. The body axis aerodynamic coefficients are computed by a transformation of the wind axis aerodynamic force and moment coefficients.

$$[\ c_{fx}\ c_{fy}\ c_{fz}]^T = T_{w/b}\,[-c_d - c_y - c_l]^T$$

$$[\ c_{mx}\ c_{my}\ c_{mz}]^T = T_{w/b}\,[\ c_r - c_m\ c_n]^T$$

where $T_{w/b}$ is the transformation from the wind to the body axis.

$$T_{w/b} = \begin{bmatrix} \cos\beta\cdot\cos\alpha & \sin\beta\cdot\cos\alpha & -\sin\alpha \\ \sin\beta & -|\cos\beta| & 0 \\ |\cos\beta|\cdot\sin\alpha & \sin\beta\cdot\sin\alpha & \cos\alpha \end{bmatrix}$$

The aerodynamic forces and moment at the reference point can then be computed from the body axis aerodynamic coefficients, the reference area and length, and the dynamic pressure.

4.2 Aerodynamic Interference

The main rotor downwash can have a significant impact on the airflow at the slung load in hover and low-speed flight, depending on the relative position of the slung load with respect to the aircraft and the sling cable configuration. With the main rotor interference on the slung load modeling capability available, the major cause of slung load spinning about its vertical axis in hover can be modeled and analyzed.

The rotor wake interference is modeled using finite state dynamic wake model. A brief discussion of the finite state dynamic wake interference model is presented here. More detailed formulations for the finite state dynamic wake interference calculation can be found in Refs. [6] and [7].

When a slung load is immersed in the rotor induced flow field, the flow field around the slung load body will be strongly affected by the rotor induced velocity. In the present study, the distribution of the main rotor induced velocity over the slung load is modeled by the finite state dynamic wake interference component implemented in FLIGHTLAB, which was developed based on an extension of the Peters-He finite state dynamic wake theory (Ref. [8]). The rotor wake interference computation using the finite state wake model is both unsteady and nonuniform.

From the finite state dynamic wake equations, the induced velocity at an arbitrary flow field point can be computed through an integration of

$$v_i = -\frac{1}{V_T} \int_{\xi}^{\infty} \Phi^V_{,i} \, d\xi \tag{1}$$

where Φ^V is the pressure function (Ref. [8]) and V_T is the rotor wake convection speed. The three components of the rotor induced velocity can then be obtained (for $i = x, y, z$) as

$$v_i = \frac{1}{2V_T} \sum_{m}^{\infty} \sum_{n}^{\infty} (q^{mc}_{in} \tau^{mcV}_{n} + q^{ms}_{in} \tau^{msV}_{n}) \tag{2}$$

where q^{mc}_{in} and q^{ms}_{in} are the induced flow influence coefficients and are related to each of the specific distributions of the rotor pressure functions (τ^{mcV}_{n} and τ^{msV}_{n}).

Based on the finite state dynamic wake theory, the above integrals are functions of the geometric relationship between the rotor and the flow field point for interference. Thus, the induced velocities obtained are both nonuniform and unsteady. In this application, the flow field points of interest are the aerodynamic computational points (ACPs) distributed over the slung load.

4.3 Unsteady Slung Load Airloads

The helicopter slung load aerodynamics is typically a blunt body flow in nature. The blunt body slung load aerodynamics are usually comprised of the following sub-components: static aerodynamics; viscous damping due to angular rates; unsteady aerodynamics of the stationary body due to vortex shedding; and unsteady aerodynamics of an oscillating body due to phase lags in separation bubbles, growth, and vortex shedding. Since the blunt slung load body involves complicated flow phenomena such as extensive flow separation, vortex shedding, etc., it is difficult to capture all the detailed flow features in a simulation. The transfer function based unsteady aerodynamic model (Ref. [9]) was implemented in the FLIGHTLAB simulation to account for the unsteady slung load aerodynamics. The transfer function coefficients were identified from the CFD results (Ref. [10]).

The transfer function for the yaw moment (C_N) and side force (C_S) can be included in a general form as

$$\frac{C_N(s)}{\Delta\beta(s)} = \frac{\left[\frac{V}{V_{ref}}\right]^2 a_2 s^2 + \left[\frac{V}{V_{ref}}\right] a_1 s + a_0}{\left[\frac{V}{V_{ref}}\right]^2 b_2 s^2 + \left[\frac{V}{V_{ref}}\right] b_1 s + b_0} \; e^{-\left[\frac{V}{V_{ref}}\right]\tau s} \tag{3}$$

For the side force, C_N was replaced by C_s and the transfer function coefficients are replaced by those for C_S. In the above equation, V and V_{ref} are the current air speed and the reference speed, respectively, and $\Delta\beta$ is the sideslip angle perturbation over a reference sideslip angle. The coefficients $b_2, b_1, b_0,\ a_2, a_1, a_0$, and the parameter τ are identified for several different reference sideslip angles at a reference speed of 60 knots. The values for the transfer function coefficients for the example slung load can be found in Ref. [10]. Generally, the transfer function coefficients will vary with the flight velocity and therefore a scale factor, V/V_{ref}, is applied to extend the model to all airspeeds. Since the quasi-steady aerodynamics are already implemented in the FLIGHTLAB model via table lookup, the model in Equation 3 is modified by replacing the a_0 term with the quasi-steady loads which are obtained via table lookup as follows:

$$C_N(s) = \frac{\left[\frac{V}{V_{ref}}\right]^2 a_2 s^2 \Delta\beta(s) + \left[\frac{V}{V_{ref}}\right] a_1 s \Delta\beta(s) + C_N^{qs}(s)}{\left[\frac{V}{V_{ref}}\right]^2 b_2 s^2 + \left[\frac{V}{V_{ref}}\right] b_1 s + b_0} \; e^{-\left[\frac{V}{V_{ref}}\right]\tau s} \tag{4}$$

where the superscript qs stands for quasi-steady. The unsteady side force, C_S, can be expressed in a similar way. To implement the above unsteady aerodynamic model in FLIGHTLAB, the pure time lag term is approximately treated as a first order lag.

In Refs. [9] and [10], the transfer functions for the yaw moment were identified at four reference sideslip angles: $\beta_0 = 0^o$, 30^o, 60^o, and 90^o. Similarly, the transfer function coefficients for the side force were identified at two reference sideslip angles: $\beta_0 = 0^o$ and 90^o. As pointed out in Refs. [9] and [10], although the behavior of the transfer function coefficients changes with the reference sideslip angle, there are nevertheless some invariants. First, the equivalent time lag (i.e., the effect of b_1 and/or τ) is approximately the same at all reference sideslip angles. In addition, the vortex shedding frequency was found to be invariant with the reference sideslip angle. To study the most important effect of the slung load unsteady aerodynamics, only the first order lead-lag model was tested in FLIGHTLAB. This first order lead-lag model can be written in a general form for both the yaw moment and side force coefficients as follows:

$$C_N(s) = \frac{\left[\frac{V}{V_{ref}}\right] a_1 s \Delta\beta(s) + C_N^{qs}(s)}{\left[\frac{V}{V_{ref}}\right] \tau s + 1} \tag{5}$$

where τ is the equivalent time lag. The side force transfer function can be expressed in a similar way using the side force coefficients. In addition, the model will be applied at all sideslip angles in the parametric study described below. This approximation neglects changes in the higher-order dynamics of the slung load unsteady aerodynamics with respect to the reference sideslip angle, but it captures the essential dynamics of the unsteady slung load motion.

In the current FLIGHTLAB helicopter-slung load configuration, the quasi-steady yaw moment and side force, which are obtained through table lookup, have already been applied to the system. Therefore, the perturbations on the yaw moment and side force due to the unsteady aerodynamics are calculated and applied to the system together with those from the existing quasi-steady model. Therefore, the perturbations can be obtained

as follows:

$$\Delta C_N(s) = C_N(s) - C_N^{qs}(s) = \frac{\left[\frac{V}{V_{ref}}\right] a_1 s \Delta\beta(s)}{\left[\frac{V}{V_{ref}}\right] \tau s + 1} - \frac{\left[\frac{V}{V_{ref}}\right] C_N^{qs}(s) \tau s}{\left[\frac{V}{V_{ref}}\right] \tau s + 1} \tag{6}$$

where the first part of the right hand side accounts for the sideslip rate, $\dot{\beta}$, and the second part accounts for the quasi-steady yaw moment passing through a first order filter. Similarly, the side force perturbation due to the unsteady aerodynamics can be obtained as the sum of two parts. It should be pointed out that, since both the unsteady yaw moment and the side force are caused by the same physical phenomenon, the denominators in the transfer functions for them should be the same.

Fig. 4 shows the predicted slung load yaw moment variation with sideslip angle at a forward velocity of 60 knots. For comparison purposes, the results from the quasi-steady model are also superimposed on the plot. From the comparisons, it can be seen that the unsteady aerodynamics creates a hysteresis loop when the side slip angle is oscillating. When the sideslip angle is increasing, the unsteady yaw moment lags behind the quasi-steady moment. Also, the maximum unsteady moment is larger than the quasi-steady value. Similarly, when the sideslip angle is decreasing, the unsteady yaw moment decreases slower than the quasi-steady yaw moment. The hysteresis behavior of the airloads will introduce a phase lag which could result in significant difference in the slung load transient response as compared to the quasi-steady airloads excitation.

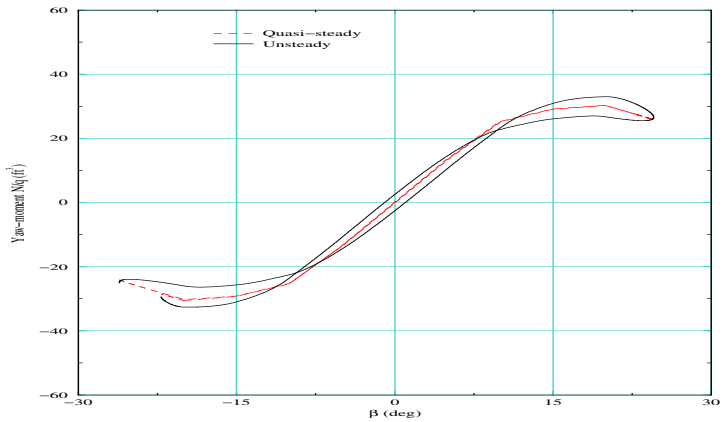

Figure 4: Slung load yaw moment variation with sideslip angle obtained using the quasi-steady model and the unsteady model, $V = 60 knots$

5 Nonlinear Trim and Control Response Solution

Another important development was to formulate an effective analysis and simulation solution algorithm for a robust rotorcraft/slung load trim, stability, and transient dynamic response analysis. The difficulty in achieving a converged solution is due to the fact that the slung load is a lightly damped dynamic system. The rotorcraft/slung load two body dynamics interaction further complicates the problem. A rotorcraft trim analysis requires that the gradient of the trim target function with respect to the controls be computed. The gradient computation is typically made by perturbing each of the controls and then integrating the rotorcraft dynamics system to steady state in order to derive the partial derivatives for constructing the trim gradient matrix. When the lightly damped slung load dynamics are involved, it becomes extremely difficult to obtain the steady state solution through time integration. One solution to this problem is to first constrain the slung load at each rotorcraft trim step and then solve the slung load steady state equilibrium using the updated rotorcraft states and controls at the end of each trim iteration. This approach has been successfully applied for multi-stage, multi-cable, and multi-hook sling load configurations through this research and development made in FLIGHTLAB.

5.1 Nonlinear Dynamics Solution

For the multi-stage cable slung load model, a 3 DOF point mass is applied to the cable connection node degrees of freedom. The three DOFs of the node introduce high frequency dynamics due to the low node mass and the high sling stiffness. This high frequency mode caused a severe solution convergence problem. To resolve this problem, a Hilber-Hughes-Taylor (HHT) algorithm, which is an extension of the Newmark-Beta method, was adopted. This algorithm provides numerical damping for the high frequency modes, yet has little effect on low frequency dynamics (Ref. [11]). The Newmark-Beta method is a second order integration scheme that is unconditionally stable for linear equations. However, nonlinearities in rotorcraft simulations, such as finite element rotor, dynamic stall, slung load models with small node masses, and the presence of high frequency modes, often drive this method to instability. The instability is more pronounced in stiffer systems with large time steps. As observed in Reference [11], instabilities usually first appear in high frequency modes while low frequency modes remain stable. Eventually, the instability grows so large that low frequency modes also become unstable. Fortunately, in most cases, the contribution of the high frequency modes to the total response is small and may be neglected. In these cases, the high frequency modes can be numerically damped and suppressed. In the case where the response of the high frequency modes are to be included, the time step must be reduced to bring the modes into the stable region.

In the HHT formulation, the system equations of motion are first modified to increase the damping of the high frequency modes and then the Newmark-Beta formulation is applied to integrate the equations. Using generalized force formulation as implemented in FLIGHTLAB, the modified equation can be written as

$$\begin{aligned} \widehat{Q} &= F_{n+1} - (M\ddot{X}_{n+1} + C\dot{X}_{n+1} + KX_{n+1}) \\ &\quad +\alpha_{hht}[(F_{n+1} - F_n) - K(X_{n+1} + KX_n)] \end{aligned} \tag{7}$$

where $\widehat{Q}$ is the generalized force in the HHT equation and is zero when the dynamic equation is at equilibrium. The modified equation also introduces α_{hht}, the HHT parameter, which is chosen such that $-\frac{1}{3} < \alpha_{hht} < 0$.

The Newmark-Beta integration equations may be written as

$$\begin{aligned} \dot{X}_{n+1} &= \dot{X}_n + a_0\ddot{X}_{n+1} + a_1\ddot{X}_n \quad (8) \\ X_{n+1} &= X_n + b_0\ddot{X}_{n+1} + b_1\dot{X}_{n+1} + b_2\ddot{X}_n \quad (9) \end{aligned}$$

Substituting Equation 9 and Equation 9 into Equation 7 yields

$$\widehat{Q}^i = -\widehat{M}\ddot{X}^i_{n+1} + (1+\alpha_{hht})F_{n+1} + g(n) \quad (10)$$

where the superscript i signifies the Newton-Raphson iteration number within a time step. $\widehat{M}$ is the effective mass matrix and is defined by

$$\widehat{M} = M + a_0 C + (1+\alpha_{hht})b_0 K \quad (11)$$

and $g(n)$ is substituted for all the terms of the previous time step, i.e.,

$$\begin{aligned} g(n) &= -\alpha_{hht}(F_n - KX_n) \quad (12) \\ &\quad -C(\dot{X}_n + a_1\ddot{X}_n) - (1+\alpha_{hht})K(X_n + b_1\dot{X}_n + b_2\ddot{X}_n) \end{aligned}$$

It is desirable to find $\ddot{X}^{i+1}_{n+1}$ such that $\widehat{Q}^{i+1} = 0$. Equation 10 then becomes

$$0 = -\widehat{M}\ddot{X}^{i+1}_{n+1} + (1+\alpha_{hht})F_{n+1} + g(n) \quad (13)$$

Subtracting Equation 13 from Equation 10 results in

$$\widehat{Q}^i = \widehat{M}\delta\ddot{X} \quad (14)$$

where

$$\delta\ddot{X} = \ddot{X}^{i+1}_{n+1} - \ddot{X}^i_{n+1} \quad (15)$$

For each iteration, the equation imbalance, $\widehat{Q}^i$, is first computed from each DOF and then $\delta\ddot{X}$ and $\ddot{X}^{i+1}_{n+1}$ are obtained from

$$\delta\ddot{X} = \widehat{M}^{-1}\widehat{Q}^i \quad (16)$$

and

$$\ddot{X}^{i+1}_{n+1} = \ddot{X}^i_{n+1} + \delta\ddot{X} \quad (17)$$

In the FLIGHTLAB implementation, iterations are performed until the equation imbalance (generalized force) $\widehat{Q}$ is driven to a convergence tolerance at each time step. The integration is then advanced to a new time step.

5.2 Two-Body Trim Algorithm

A robust two-body algorithm was developed for the coupled rotorcraft/slung load model trim analysis. Using the two-body trim algorithm, the two-body simulation models can be trimmed for an arbitrary configuration. For the helicopter/slung load configuration, the slung load is first trimmed while the helicopter body states are frozen. Once the slung load is trimmed, the resulting cable forces are applied to the aircraft slung load attachment points as constraints for the helicopter trim. The convergence of the two-body trim solution is achieved via relaxed iterations.

A dedicated solution method was introduced for the slung load model group within the helicopter/slung load solution architecture. The implemented slung load solution component allows for perturbing the equations of motion for the slung load model independently from the aircraft model in order to compute the generalized forces for the slung load trim. To do this, the solution component assembles the following slung load equations of motion:

$$\widehat{Q} = \sum F - (M\ddot{X} + C\dot{X} + KX) \tag{18}$$

where $\widehat{Q}$ are the generalized forces and moments and $\sum F$ denotes the sum of all external forces and moments. M, C, and K are the slung load system mass, damping, and stiffness matrices, respectively. For the slung load trim, the slung load displacement and orientation, X, are utilized as trim variables. The translational and rotational velocities, $\dot{X}$, are set by test conditions prior to the trim. In the current slung load trim algorithm implementation, the accelerations, $\ddot{X}$, are utilized as the trim targets, which can be trimmed to a desired value which is zero for most trim applications. The slung load trim applies the following Newton method with relaxation:

$$X^{k+1} = X^k - \omega_k [D\ddot{X}(x^k)]^{-1} \cdot \ddot{X}(x^k) \quad (k = 0, 1, ...) \tag{19}$$

where ω_k is the relaxation factor and $[D\ddot{(}x^k)]$ is the gradient matrix defined as

$$[D\ddot{X}(x^k)] = \begin{bmatrix} \frac{\partial \ddot{x}_1(x^k)}{\partial x_1} & \frac{\partial \ddot{x}_1(x^k)}{\partial x_2} & \cdots & \frac{\partial \ddot{x}_1(x^k)}{\partial x_n} \\ \frac{\partial \ddot{x}_2(x^k)}{\partial x_1} & \frac{\partial \ddot{x}_2(x^k)}{\partial x_2} & \cdots & \frac{\partial \ddot{x}_2(x^k)}{\partial x_n} \\ \vdots & \vdots & \vdots & \vdots \\ \frac{\partial \ddot{x}_n(x^k)}{\partial x_1} & \frac{\partial \ddot{x}_n(x^k)}{\partial x_2} & \cdots & \frac{\partial \ddot{x}_n(x^k)}{\partial x_n} \end{bmatrix} \tag{20}$$

The slung load trim variables, X, are numerically perturbed in order to compute the gradient matrix. The relaxation parameter, ω_k, is updated using an intelligent relaxation procedure. The highly nonlinear slung load problem may result in ill-conditioned gradient matrices. Thus, two options were added to the basic formulation to assist the trim analysis. One is to introduce a κ factor to the off-diagonal elements of the gradient matrix in order to reduce the cross-coupling effects. The other is to adopt a damping factor, μ, to remove the singularities or to overcome the ill-conditioned matrices. Thus, the enhanced Newton method for the slung load model reads as follows:

$$X^{k+1} = x^k - \omega_k [D\ddot{X}(x^k) \cdot \Gamma + \mu I]^{-1} \cdot \ddot{X}(x^k) \quad (k = 0, 1, ...) \tag{21}$$

where

$$\Gamma = \begin{bmatrix} 1 & & & \kappa & \\ & 1 & & & \\ & & 1 & & \\ & \kappa & & 1 & \\ & & & & 1 \end{bmatrix} \tag{22}$$

The default values for μ and κ are $\mu = 0.0$ and $\kappa = 1.0$, respectively. They can be adjusted for specific applications.

The slung load trim algorithm described above was implemented in FLIGHTLAB such that its results are incorporated in the equations used to calculate the rotorcraft trim constraints. In the implementation, the slung load model is first initialized for the sling cable to be statically fully stretched.

The slung load configuration may include cable connection nodes with translational degrees of freedom which are needed for multi-stage sling cable configurations. Multiple external slung load hooks may also be specified. The trim variables and targets are assembled when the model is loading in order to include all degrees of freedom of the slung load configuration. For models with the swivel components, the swivel DOF and the slung load yaw attitude cannot be used as trim variables at the same time. Also, for configurations with multiple hooks, the slung load initialization scheme may be invoked if the sling cable tensions are detected to be zero during the trim.

5.3 Stability Analysis

The helicopter/slung load stability analysis was performed through the model linearization and the eigenvalue calculation on the stability matrix generated from the linearization on the nonlinear simulation. The linearization utility can be configured to generate either a full linearized helicopter/slung load model or a reduced order state space model as desired. For most handling qualities analysis applications, an eight state model, which includes three body translational and three angular motion and vehicle pitch and roll attitudes, is typically desired. A quasi-static model reduction technique is adopted under this analysis by selecting the dynamically retained states as specified.

Two linearization algorithms are provided by the linear analysis utility. One is the so called "averaged genq" method, which extracts stability, control, and output matrices by making perturbations at each rotor azimuth, collecting the resulting perturbed generalized forces accordingly, and then averaging the resulting partial derivatives over one rotor revolution. The "averaged genq" method is very accurate if the dynamic system does not contain any implicit states. Unfortunately, this is usually not the case for rotorcraft models.

To overcome the hidden state hurdle, the "steady state perturbation" solution is adopted which obtains the linear model by perturbing the state or control, integrating the model to steady state, and then averaging the resulting partial derivatives over rotor revolutions. Under the "steady perturbation" approach, the effect of all hidden states, such as that found in a "delay" component, etc., will be effectively accounted for in the resulting linearized model. The difficult side of the approach is the proper selection of the perturbation size used in the partial derivative calculation through the "steady state"

run. Too large a perturbation size will step beyond the linear range of the model equilibrium state and result in an error. Too small a perturbation size will, on the other hand, produce erroneous results due to the steady state convergence tolerance.

6 Results and Discussion

A simulation evaluation was conducted to validate the FLIGHTLAB rotorcraft/slung load model. The simulation validation was made for a FLIGHTLAB UH-60L helicopter with an external slung load. The UH-60L/slung load configuration is modeled using FLIGHTLAB aerodynamic, structural, propulsion, and control components. Simulations were carried out for the trim, transient responses, and stability analyses to examine the simulation model behavior compared to the flight test measured data (Ref. [5]). Figure 2 shows the two stage slung load model used in the simulation validation.

6.1 Trim and Periodic Slung Load Motion

Figure 5 presents the comparison of the trimmed control stick positions against the flight test data. The simulation correctly predicts both the variation trend and magnitude. Figure 5 also shows the variation of the trimmed helicopter pitch and roll attitudes with flight speed. It can be seen that the simulation well correlates with the flight test data as well.

To trim a helicopter/slung load configuration, the helicopter body is usually trimmed to a condition with an averaged zero acceleration while the slung load is allowed to move freely during the helicopter trimming procedure in practical flight test. The slung load motion during the flight test trimming can be viewed as a periodic steady state. To validate the helicopter/slung load responses to pilot control stick input during the steady state trim, the time histories of the trim stick positions from the flight test are used to drive the FLIGHTLAB model. The purpose of doing this is to excite the periodic motion of the slung load to be close to the motion during the flight test.

Figure 6 shows the simulated aircraft pitch, roll, and yaw rate response driven by the control stick inputs from the flight test during the helicopter trimming procedure at a forward flight speed of 95 knots. Figure 7 shows the corresponding slung load longitudinal and lateral swing angle variations with time due to the same control inputs. As seen, the aircraft pitch and roll rate responses to the stick input correlate very well with the flight test data. The simulated yaw rate response follows the trend of the flight test data. But, the prediction seems to be lack of higher frequency variation and there are also phase discrepancies which could be due to the possible model deficiency in cross-axis coupling. As for the slung load response, the simulation accurately predicts both the magnitude and the phase as compared to the flight test measured data.

6.2 Transient Responses

The helicopter/slung load response to a one inch longitudinal stick doublet input at a forward flight speed of 95 knots is shown in Figure 8. For comparison purposes, the corresponding flight test data are superimposed on the plots. From Figure 8, it can be

seen that the both the pitch and roll rate response to the longitudinal doublet input correlates very well with the flight test data. The model was further validated at several other flight speeds. Similar good correlations with the flight test data were also obtained.

The UH-60L/slung load model was further validated in the frequency domain. The simulated frequency responses for the helicopter body and slung load to the pilot control stick sweep inputs were compared with the corresponding flight test results. The frequency responses were extracted from the response time histories by using the FLIGHTLAB's multi-input single-output nonparametric identification tool. For the results presented here, a window size of 2048 points was used.

The first case examined was the helicopter body rate frequency responses to pilot control sweep in hover. Figures 9 and 10 present the helicopter body pitch and roll rate frequency responses to the longitudinal cyclic stick sweep input and the simulation results were compared with the corresponding flight test data also. From the comparison, it can be seen that the predicted pitch and roll rate frequency responses in hover match well with the flight test results, except for the phase of the off-axis roll rate response to the longitudinal stick input which may be caused by the rotor wake distortion effect as discussed in Ref [12].

The next case investigated was the helicopter response to control sweep in forward flight. Figure 11 shows that the simulated helicopter pitch rate frequency response to the longitudinal stick input at 60 knots, including comparisons with the flight test results. The frequency responses are expressed in terms of magnitude, phase, and coherence. From Figure 11, which is the on-axis pitch rate frequency response to the longitudinal cyclic stick input, it can be seen that the FLIGHTLAB simulation correlates well with the flight test results in both magnitude and phase. Figure 12 shows the predicted helicopter body roll rate frequency responses to the lateral cyclic stick input at 60 knots, including comparisons with the corresponding flight test results. Similar good agreement between the predicted and measured frequency response was achieved.

6.3 Stability Analysis

To investigate the influence of the slung load on the stability of the helicopter, the FLIGHTLAB helicopter/slung load model was linearized and the eigenvalues of the linearized model were obtained. Due to the complexity of the slung load mode, the linearized model was obtained via numerical perturbation. To identify the effects of the slung load, the linearizion was made for three reduced order models.

- Baseline: The baseline model (Model I) does not have the slung load. The baseline reduced model contains 8 body states, i.e., $u, w, q, \theta, v, p, r, \phi$.

- Helicopter/Slung Load (Model II): The reduced model includes only the 8 body states. But, all the slung load DOFs were quasi-statically reduced.

- Helicopter/Slung Load (Model III): The reduced model includes both the 8 states for the body and 2 DOFs for the slung load (longitudinal and lateral swing).

All the linearizations performed used a perturbation step size $\Delta = 0.02$ and a convergence tolerance $\epsilon = 0.0005$. Figure 13 shows the comparisons of the eigenvalues of the linearized

model with reduced orders. In the linearized baseline model (Model I), which retains 8 DOFs for the body, the pitch, roll, heaving, and spiral subsidences as well as the phugoid and dutch roll modes can be clearly identified as shown in Figure 13. It can also be seen that the phugoid mode in the baseline model is slightly unstable in hover. When the slung load is included but all the slung load states are reduced (Model II), it is noticed from Figure 13 that the slung load significantly changes the stability characteristics of the helicopter when compared with the baseline model. The phugoid mode in the slung load model becomes stable because of the fact that the slung load hook position is ahead of the aircraft C.G. It can also be seen that, while the pitch and heaving subsidences are well separated in the baseline model, they are fully coupled and form an oscillatory pair in the slung load model in hover. In addition, the eigenvalues for the next level linearization (Model III), which retains the load longitudinal and lateral swing angles, are superimposed on Figure 13. The comparisons between the results for Model II and Model III, it can be seen that retaining 2 DOFs for the slung load swing motion does not significantly change the stability characteristics of the slung load model in hover. The main effect of retaining the load DOFs is a slight change in the frequency of the oscillatory modes (phugoid, dutch roll, and coupled pitch/heaving).

The linearization at 60 knots is considered next. Figure 14 shows the comparisons of the eigenvalues of the linearized models at three different levels. Similar to the hover case, in the linearized baseline model, which retains 8 DOFs for the body, the pitch,roll, heaving and spiral subsidences as well as the phugoid and the dutch roll modes can still be clearly identified as shown in Figure 14. However, unlike in the hover case, where the pitch and roll are uncoupled, the pitch and roll motion here become significantly coupled and form a pair of oscillatory eigenvalues in the linearized slung load model (Model II) which reduces all the slung load DOFs. In addition, the damping of the coupled pitch/roll mode is significantly less than either the pitch or roll subsidence in the baseline model. It can also be seen from Figure 14 that reducing all the load DOFs does not significantly change the stability characteristics of the helicopter when compared to the linearization results of Model III which retains two DOFs for the slung load swing motion.

7 Concluding Remarks

Efforts were made to develop a rotorcraft sling load modeling and simulation capability in FLIGHTLAB. The simulation was validated against available flight test data for a UH-60L/slung load configuration. The simulation development and validation showed that the FLIGHTLAB helicopter/sling load modeling and analysis tool can effectively predict the helicopter performance and transient response under the influence of sling loads. The simulation tool can also reasonably predict the sling load dynamic response in terms of both longitudinal and lateral swing motion. The FLIGHTLAB helicopter/sling load modeling and analysis tool was further tested for stability analysis. It was shown that the tool can be effectively applied for linearized model development for sling load stability analysis and control design applications in both hover and forward flight.

The FLIGHTLAB rotorcraft sling load modeling tool development showed that a geometrically exact multi-body formulation for rotorcraft/slung load dynamics is essential for an accurate control response prediction. Also, unsteady slung load aerodynamics are

required in order to properly simulate the transient motion of the slung load. For a sling load configuration that involves any high frequency node DOF such as that found in a two-stage sling load configuration, an advanced simulation integration algorithm, such as HHT, is required in order to improve the solution convergence. Trimming the rotorcraft/slung load dynamic system is a demanding task. The two-body trim algorithm developed in FLIGHTLAB has proved to be very effective.

8 Acknowledgments

This research was sponsored by US Army under the contract No. DAAH10-03-C-0001 and Mr. Kristopher Strope was the technical monitor.

References

[1] Cicolani, L.S. and Kanning, G., "Equations of Motion of Slung-Load Systems, Including Multilift Systems," NASA TP 3280, 1992.

[2] Stuckey, R.A., "Mathematical Modeling of Helicopter Slung-Load Systems," DSTO-TR-1257, 2001.

[3] Cicolani, L.S.; Sahai, R.; and Tucker, G., et al, "Flight Test Identification and Simulation of a UH-60A Helicopter and Slung Load," NASA/TM-2001-209619, 2001.

[4] Advanced Rotorcraft Technology, Inc., "FLIGHTLAB Theory Manual," March 2004.

[5] Gassaway, Bryan; Strope Kristopher; Luigi Cicolani Luigi; Lusardi, Jeff; He, Chengjian and Robinson Dwight, "Predictive Capabilities of a UH-60 FLIGHTLAB Model with an External Sling Load," 62nd AHS Forum, Phoenix, Arizona, May 9-11, 2006

[6] He, Chengjian, "Finite State Dynamic Wake Interference Modeling for Rotorcraft Simulation," Proceedings of the 53rd American Helicopter Society Forum, Virginia Beach, VA, April 1997

[7] He, Chengjian; Xin, Hong; and Bhagwat, Mahendra, "Advanced Rotor Wake Interference Modeling for Multiple Aircraft Shipboard Landing Simulation," 60th American Helicopter Society Forum, Baltimore, Maryland, June 2004.

[8] Peters, D. A. and He, Chengjian, "Finite State Induced Flow Models Part II: Three Dimensional Rotor Disk," **Journal of Aircraft**, Vol. 32, No. 2, March-April, 1995

[9] Cicolani, L.S.; Tischler, M.B.; et al, "Unsteady Aerodynamic Model of a Cargo Container for Slung-Load Simulation," The Aeronautical Journal of the Royal Aeronautical Society, July 2004.

[10] Cicolani, L.S.; Tischler, M.B.; et al, "Unsteady Aerodynamic Model of a Cargo Container for Slung-Load Simulation: Preliminary Aerodynamic Data and Model Identification," NASA TP 2004-212817.

[11] Hilber, H. M.; Hughes, T. J. R.; and Taylor, R. L., "Improved Numerical Dissipation for Time Integration Algorithms in Structural Dynamics," Earthquake Engineering and Structural Dynamics, Vol 5, 1977, pp. 283-292.

[12] He, Chengjian; Goericke, Jan; and Kang, Hao, "Modeling Enhancements for Physics-Based Simulation Validations," Proceedings of the 61st AHS Forum, Grapevine, TX, June 2005.

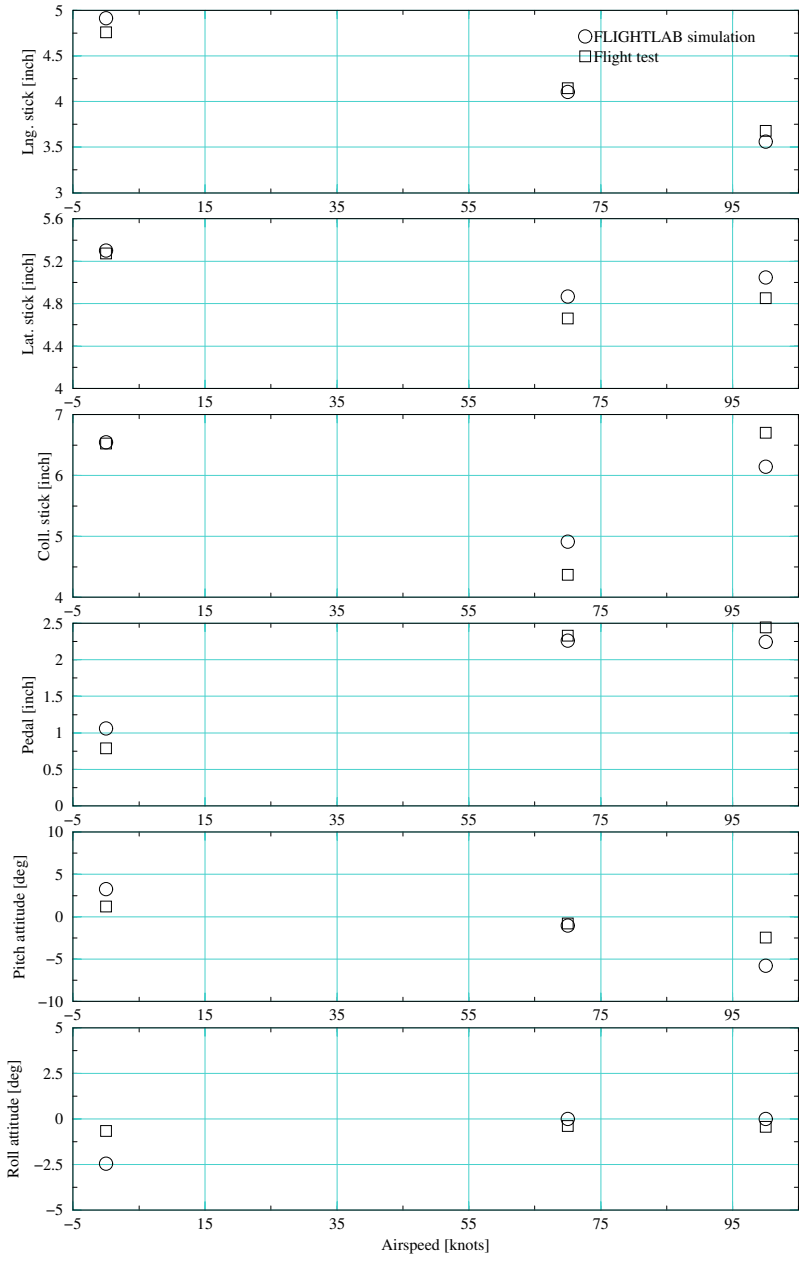

Figure 5: Predicted trim stick position and aircraft attitudes as compared to measured data

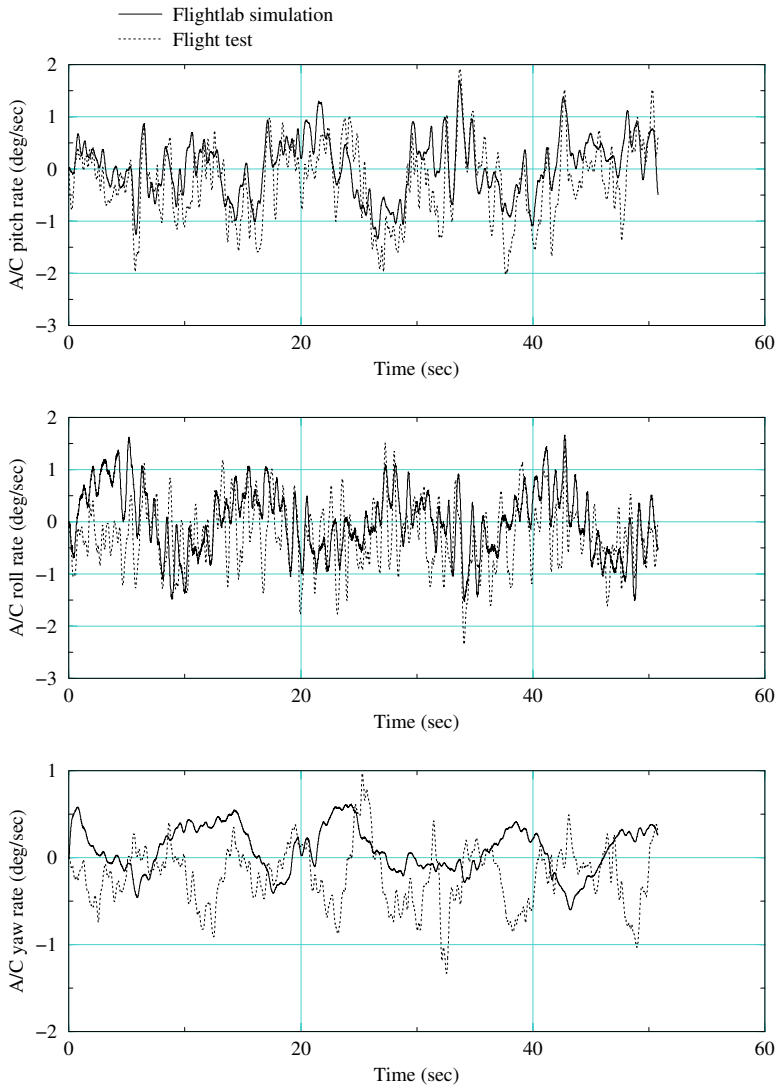

Figure 6: Predicted transient aircraft motion as compared to measured data at 95 Knots

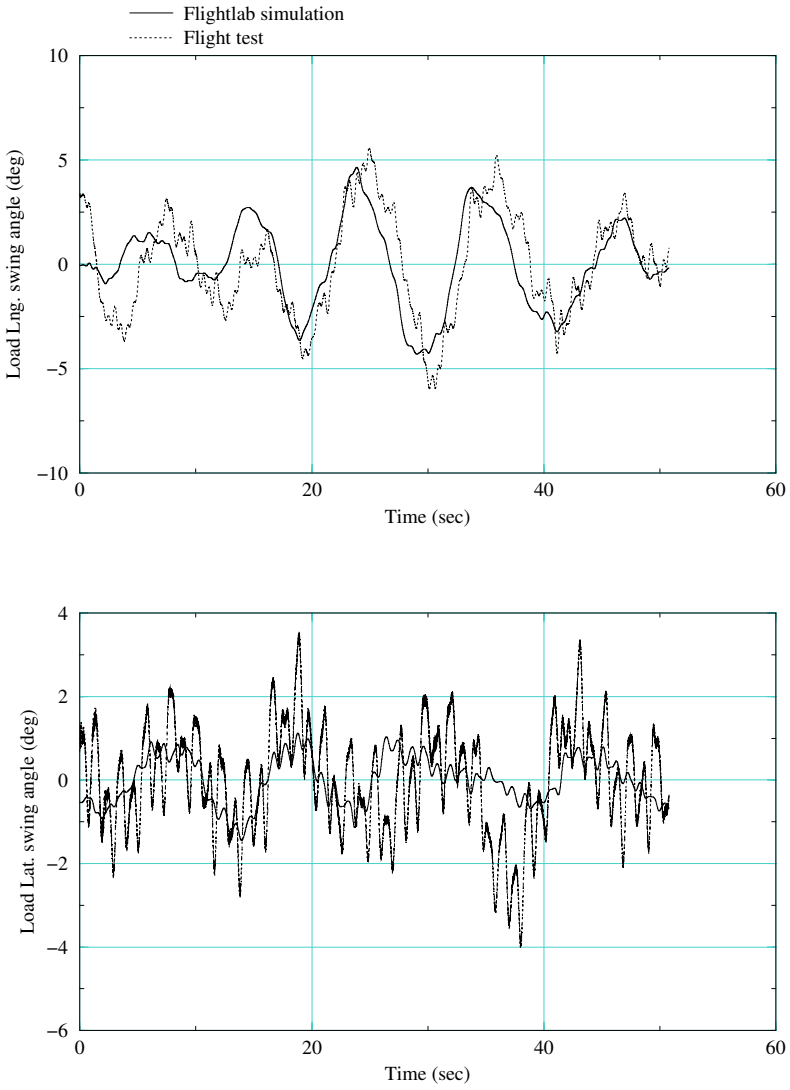

Figure 7: Predicted transient slung load motion as compared to measured data at 95 Knots

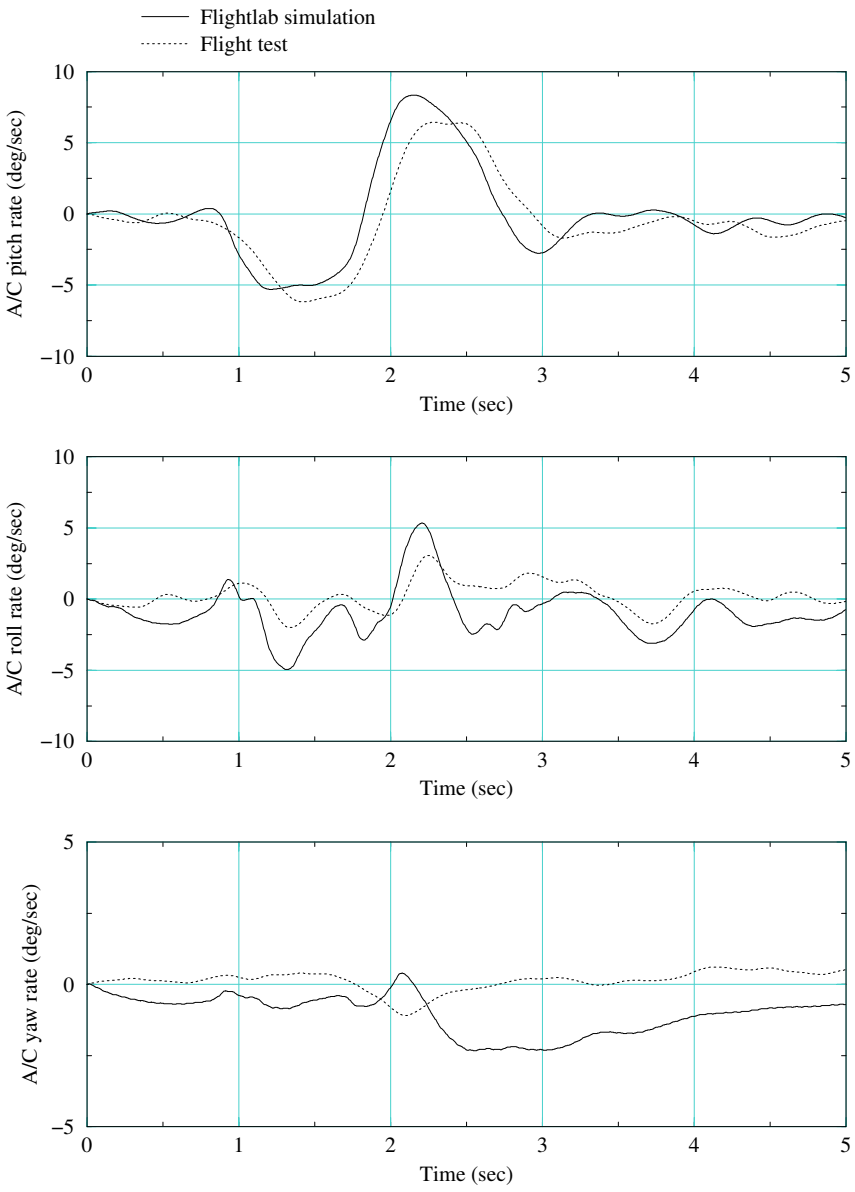

Figure 8: Helicopter responses to a one inch longitudinal doublet at 95 knots

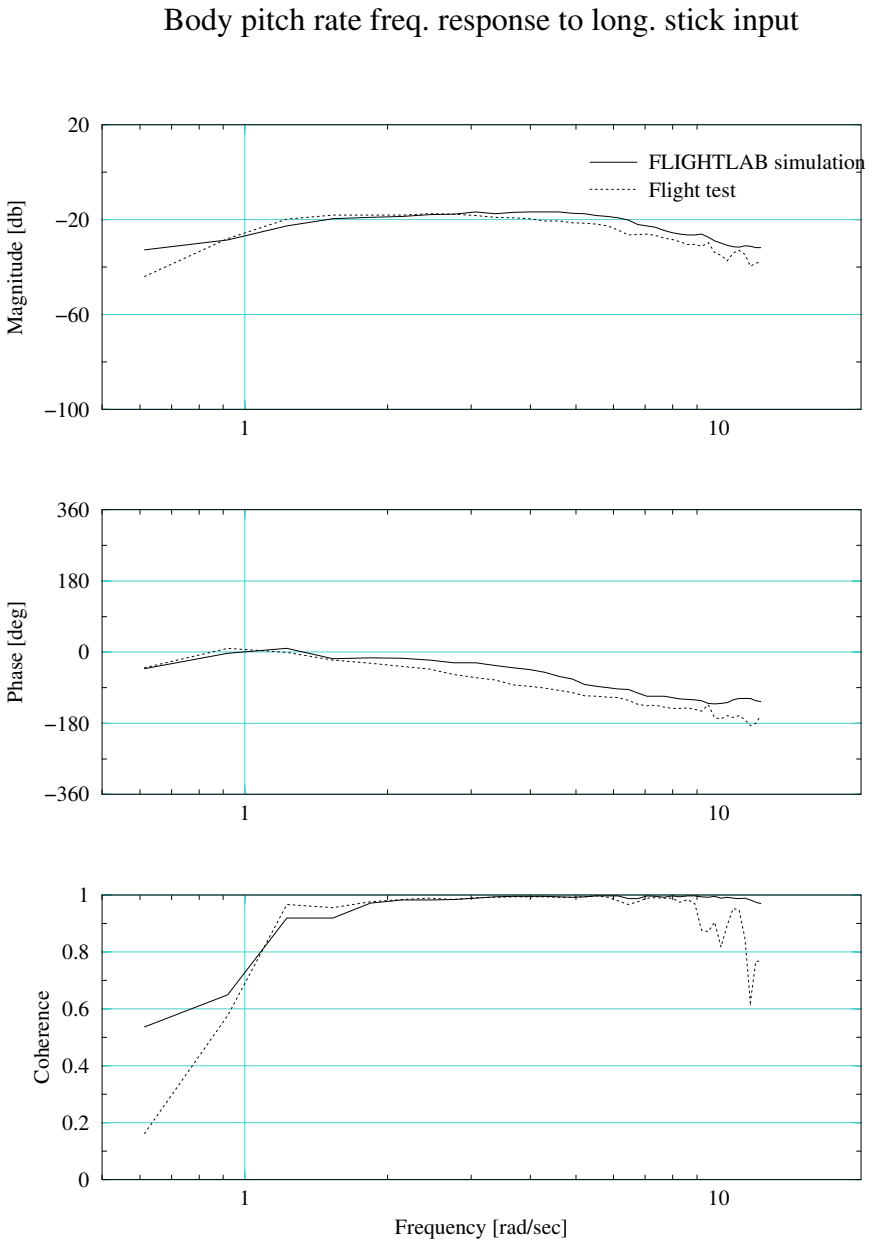

Figure 9: Pitch rate frequency response to longitudinal stick input in hover

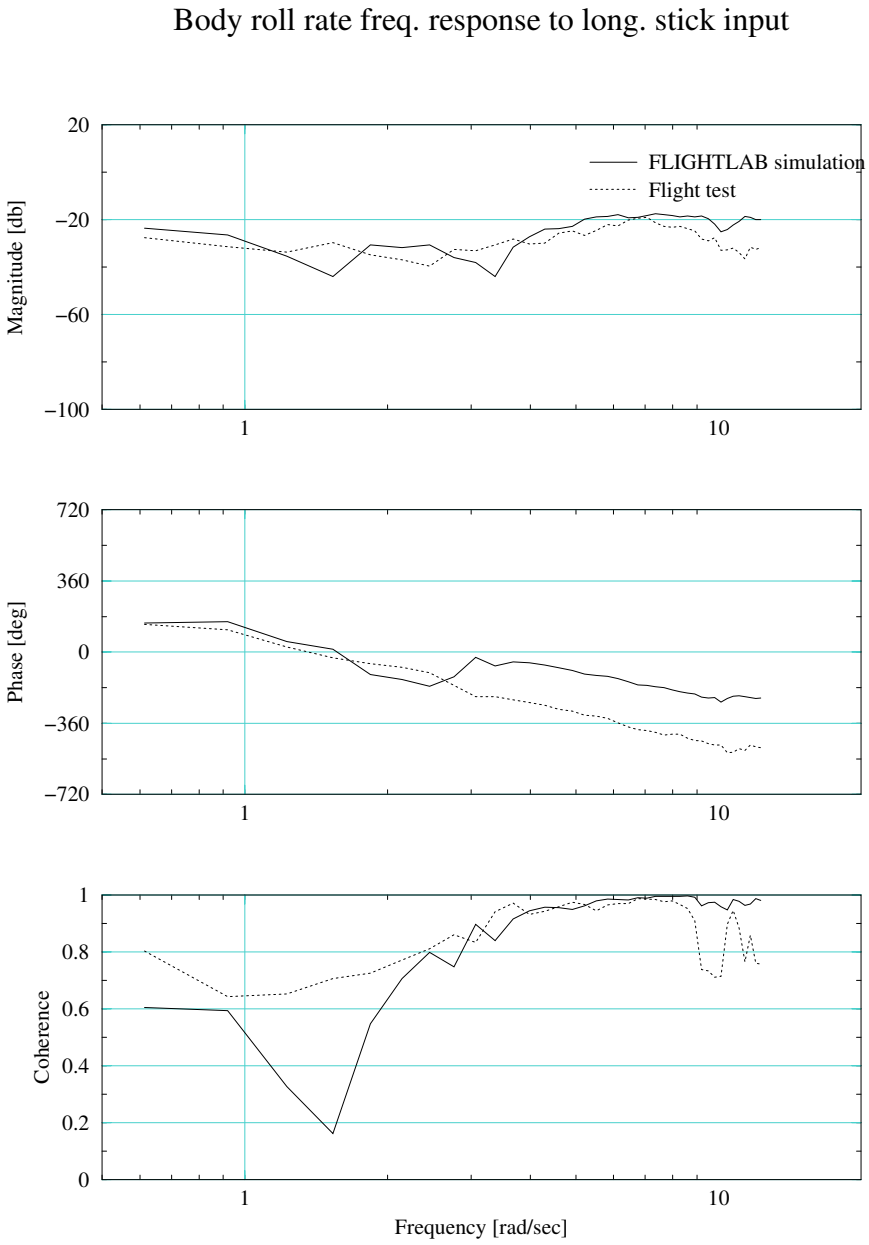

Figure 10: Roll rate frequency response to longitudinal stick input in hover

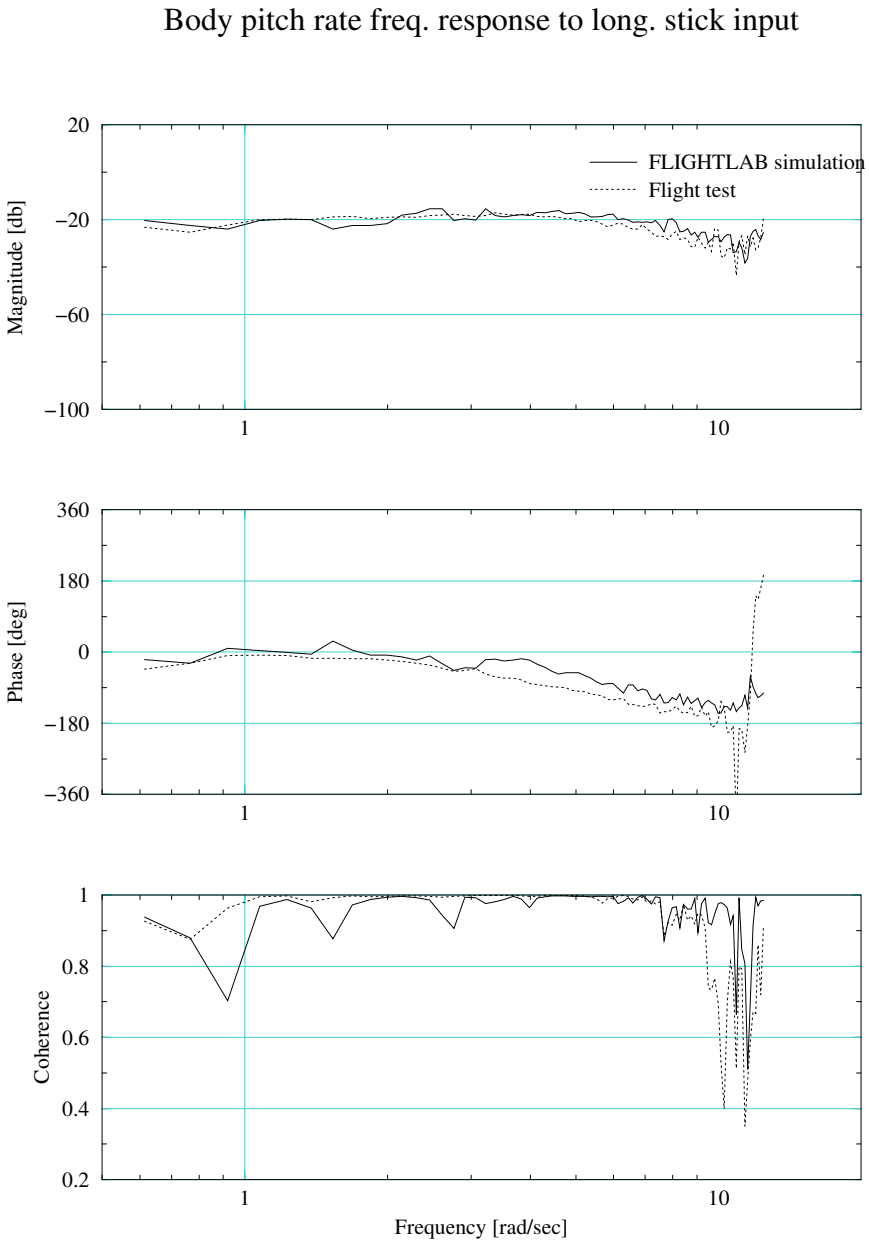

Figure 11: Pitch rate frequency response to longitudinal stick input at 60 knots

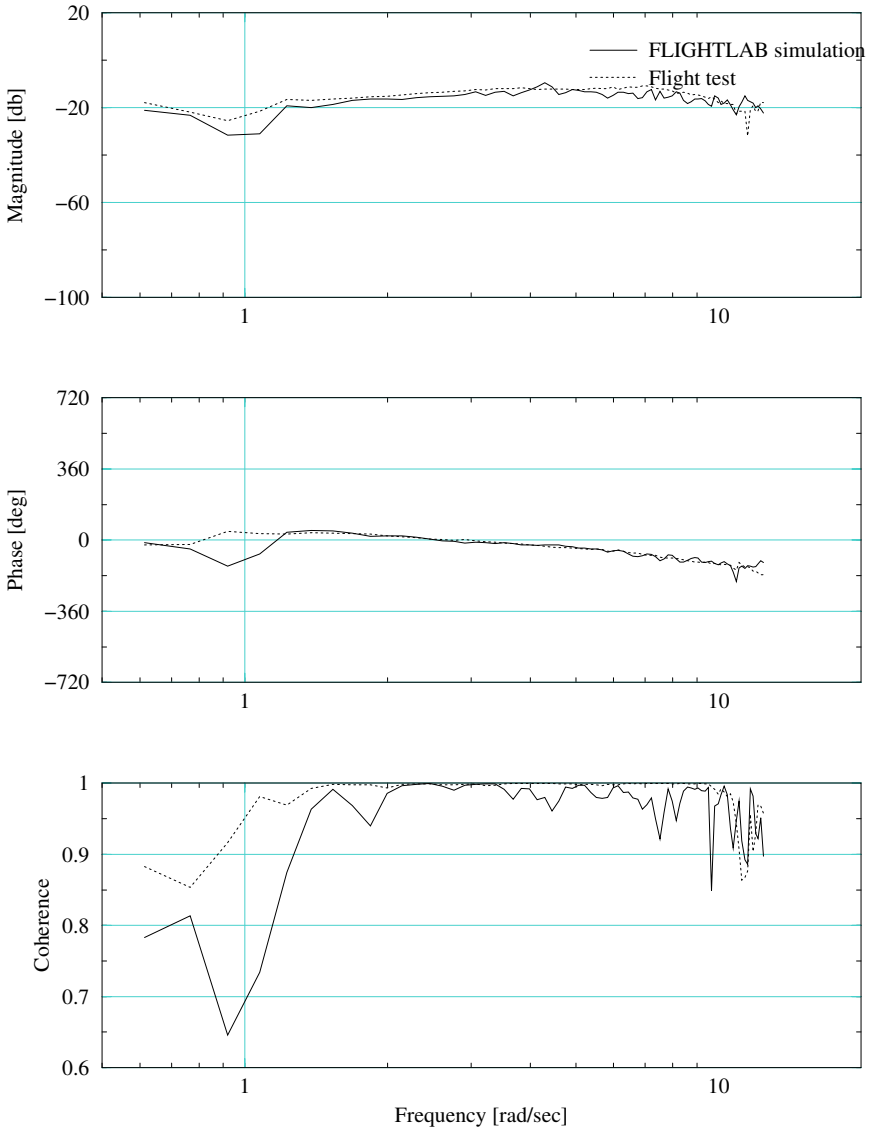

Figure 12: Roll rate frequency response to lateral stick input at 60 knots

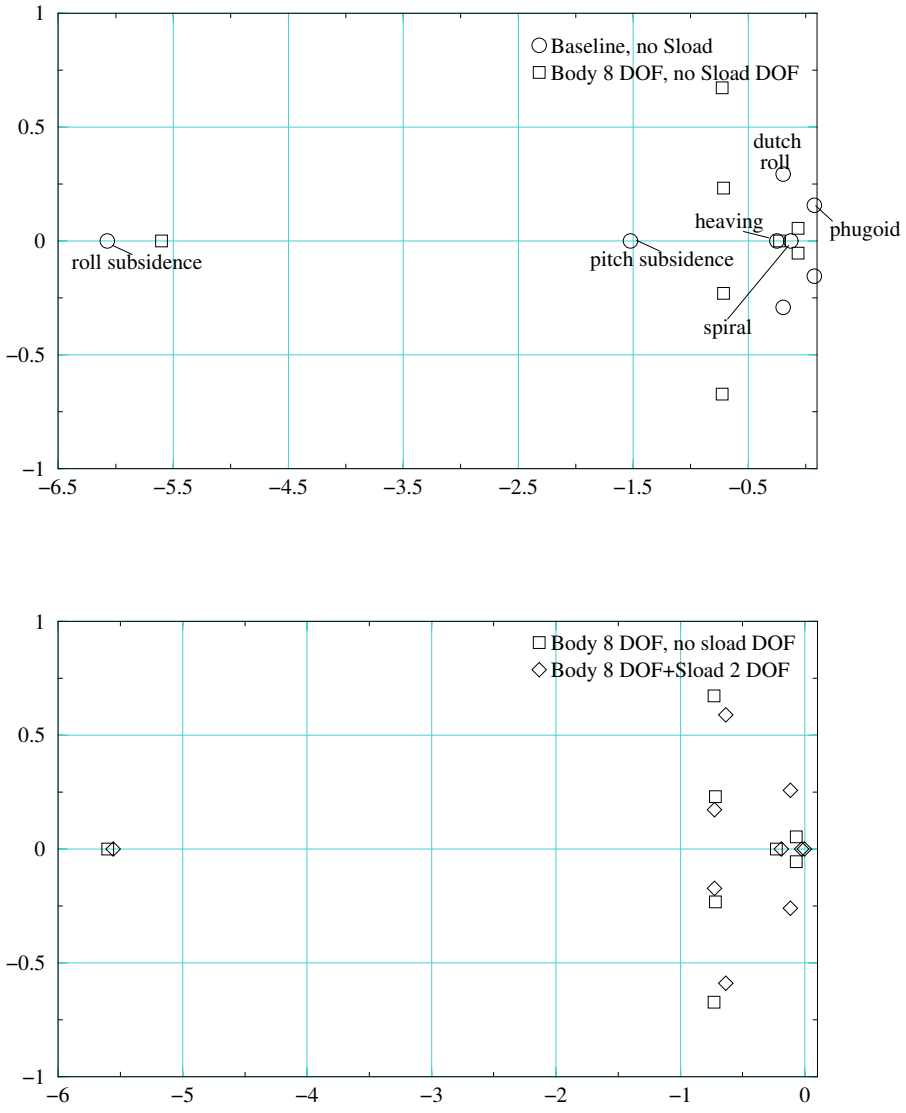

Figure 13: Eigenvalues of the linearized helicopter/slung load models in hover

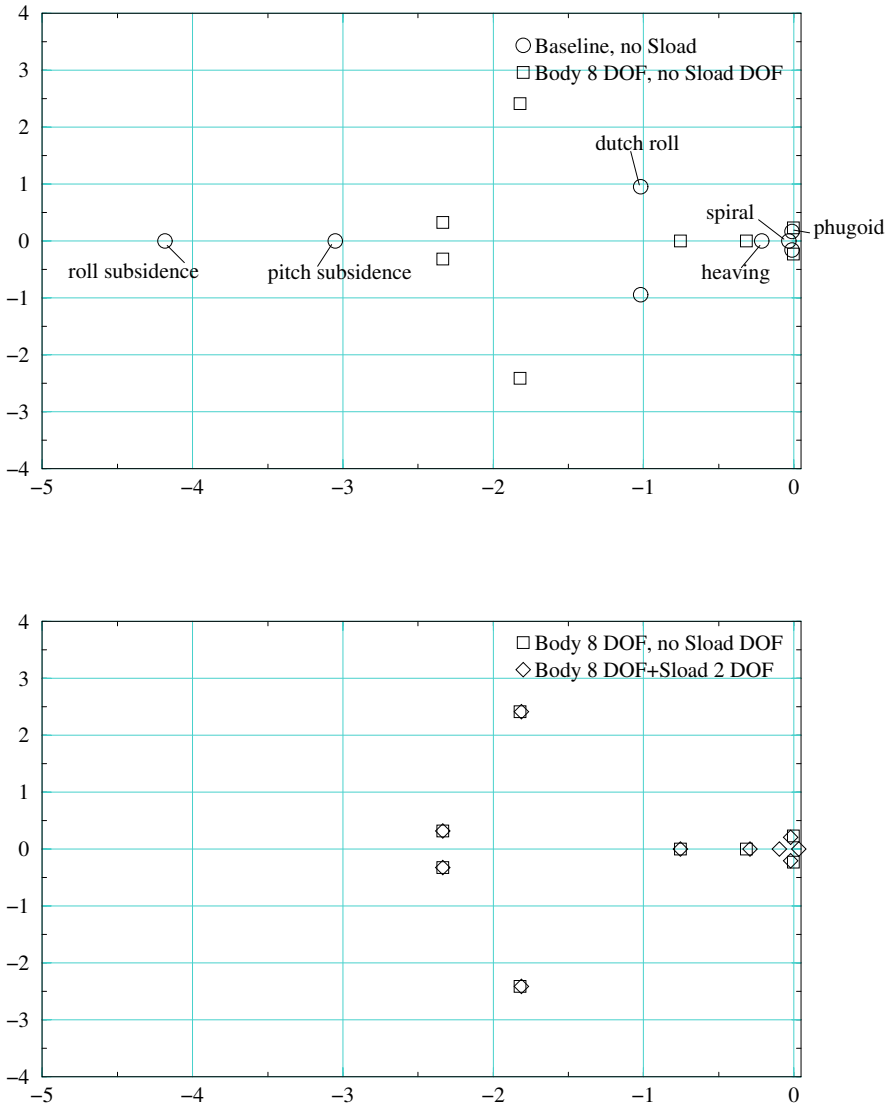

Figure 14: Eigenvalues of the linearized helicopter/slung load models at 60 knots